

Article

A Distance Detector with a Strip Magnetic MOSFET and Readout Circuit

Guo-Ming Sung *, Wen-Sheng Lin and Hsing-Kuang Wang

Department of Electrical Engineering, National Taipei University of Technology, Taipei 10608, Taiwan; wensheng.0@gmail.com (W.-S.L.); krs@ms15.hinet.net (H.-K.W.)

* Correspondence: gmsung@ntut.edu.tw; Tel.: +886-2-2771-2171 (ext. 2121); Fax: +886-2-2731-7187

Academic Editors: Nian X. Sun, Ming Liu and Menghui Li

Received: 17 November 2016; Accepted: 4 January 2017; Published: 10 January 2017

Abstract: This paper presents a distance detector composed of two separated metal-oxide semiconductor field-effect transistors (MOSFETs), a differential polysilicon cross-shaped Hall plate (CSHP), and a readout circuit. The distance detector was fabricated using 0.18 μm 1P6M Complementary Metal-Oxide Semiconductor (CMOS) technology to sense the magnetic induction perpendicular to the chip surface. The differential polysilicon CSHP enabled the magnetic device to not only increase the magnetosensitivity but also eliminate the offset voltage generated because of device mismatch and Lorentz force. Two MOSFETs generated two drain currents with a quadratic function of the differential Hall voltages at CSHP. A readout circuit—composed of a current-to-voltage converter, a low-pass filter, and a difference amplifier—was designed to amplify the current difference between two drains of MOSFETs. Measurements revealed that the electrostatic discharge (ESD) could be eliminated from the distance sensor by grounding it to earth; however, the sensor could be desensitized by ESD in the absence of grounding. The magnetic influence can be ignored if the magnetic body (human) stays far from the magnetic sensor, and the measuring system is grounded to earth by using the ESD wrist strap (Strap E-GND). Both ‘no grounding’ and ‘grounding to power supply’ conditions were unsuitable for measuring the induced Hall voltage.

Keywords: distance detector; Hall effect; strip MAGFET; polysilicon cross-shaped Hall plate; magnetic sensor; readout circuit; difference amplifier; instrumentation amplifier

1. Introduction

The Hall plate is a major magnetic sensor, which is fabricated using CMOS technology, for sensing the magnetic induction perpendicular to the Hall plate surface and converting it into a corresponding electrical signals such as voltage, current, and frequency [1–3]. To enhance the linear characteristics of a current-mode Hall sensor, various compensated techniques have been developed [4–6]. The Hall plate performs with low-voltage-related magnetosensitivity compared with a magnetotransistor or magnetic MOSFET (MAGFET) [7]. A split-drain MAGFET is widely used as a Hall sensor for sensing the magnetic induction perpendicular to the MAGFET plane, in which a current difference is obtained between two adjacent drains of the MAGFET [8]. The relative sensitivity depends on the primary geometric parameters and biasing conditions of the applied magnetic device [9,10]. A symmetrical and differential structure performs with effective sensitivity [8]. In addition, the strip approach is considered to transmit a biasing current of up to 500 mA, whereas in the coil approach, the biasing current is limited to 20 mA [11]. The strip MAGFET with two sources is superior to that with a shared source in terms of the biasing current. In the present study, CSHP was used to detect the applied magnetic induction and to induce the differential Hall voltages, which was connected to two gates of two separated MOSFETs and generated two separated drain currents. An output voltage was obtained using a readout circuit. Notably, the magnetosensitivity was enhanced because the drain current of the

MOSFET was a quadratic equation of the induced Hall voltage, which was equal to the gate voltage of the MOSFET, and the offset voltage will be effectively eliminated by the differential topology of the CSHP [12].

Magnets and magnetic induction sensing devices are often attractive in instrumentation because they can be operated in noncontacting conditions and are small in size [13]. However, the magnetic induction decays with distance according to the power-law relationship. A magnetic induction sensing device with a high sensitivity to small magnetic induction and linear response to human motion should be selected [13]. Notably, the magnetic induction strength is in the order of tens of Gauss. The proposed device in [13] could be useful in situations that require noncontacting displacement measurements. In addition, a linear bidirectional moving-magnet actuator with elastic magnetic force was presented in [14], which is an arrangement of two linear radiometric Hall sensors and a small permanent magnet disc attached to the mobile actuator's rod that moves between the two fixed sensors. An open-loop method, proposed by Arcire [14], uses an analog flux density transducer based on the Hall effect with a microcontroller board for acquiring and processing the analog data delivered by the transducer. The determination of the displacement around a neutral equilibrium position is easy. Moreover, Netzer described two linear methods for noncontacting position measurement based on a relative movement between a Hall-element magnetic sensor and contact gradient static magnetic induction [15]. The induction intensity at the edges of the linear range was approximately ± 300 G, and the maximum error due to the earth's magnetic induction of ± 0.3 G was approximately 0.1%. In addition, a new position detecting system by using the magnetic flux of the magnet on the mover was proposed, in which a Hall element was considered in a flux sensor for a synchronous motor [16]. Moreover, an intelligent odometer was studied using the Hall effect to avoid the mechanical odometer defect. The speed and mileage were measured using the Hall sensor through the pulse detection method [17].

For distance detection, an unconventional method was proposed to identify the lane markings on a road surface through laser measurement system. This method was achieved using the reflection of the laser beam [18]. Fall detection in elderly residents was performed using an infrared distance sensor [19]. Furthermore, the Poisson distance image was acquired by solving the two-dimensional Poisson equations defined on the spatial-temporal accumulative image, and the action descriptors were fed into the nearest neighbor classifier to recognize daily actions, particularly to detect the abnormal fall action [20]. In addition, an advanced driver assistance was presented to complete the measurement of the distance between a vehicle and the detected object. Particular attention has been given to the vision-based technique because it is considered one of the most accurate systems for identifying targets and measuring the distance from the target to the vehicle [21]. In brief, distance measurement can be completed using techniques such as laser beam, infrared sensor, visual-based fall detection, and vision-based technique. However, both laser beam and infrared sensor are oriental sensors, and the visual-based fall detection and vision-based technique operate in a bright environment. The object to be measured cannot be detected if it is located in the dark or has diverged from the oriental range even when it is considerably closer to the sensor. To resolve these faults, the current study proposes a distance detecting method by using the strip MAGFET, which includes two separated MOSFETs, a differential polysilicon CSHP, and a readout circuit.

The proposed distance detector could detect the distance from the magnetic body (human) to the magnetic sensor by sensing the magnetic induction of the magnetic body perpendicular to the chip surface. The strip MAGFET not only increased the magnetosensitivity but also eliminated the offset voltage which is generated because of the device mismatch and Lorentz force [22]. Moreover, a commercial instrumentation amplifier (IA) INA333 was applied to amplify the output voltage of the readout circuit and increase the detecting distance. The remainder of this paper is organized as follows. Section 2 describes the operational principles of the proposed distance detector. Section 3 presents the readout circuit for the distance detector. Section 4 presents some simulated and measured results. Section 5 presents discussion followed by conclusions.

2. Operational Principles of the Distance Detector

Figure 1 presents a strip MAGFET, which is composed of two separated MOSFETs, M1 and M2, and a differential polysilicon CSHP, for sensing the magnetic induction B_Z perpendicular to the chip surface. The distance from the magnetic body (human) to the magnetic device (strip MAGFET) can be easily detected using the proposed magnetic sensor. I_{bias} is the biasing current in the y -direction and F_{-x} is the Lorentz force in the x -direction, reversely. The differential topology not only effectively cancels the offset but also doubly enhances the magnetosensitivity. A polysilicon CSHP is located on two identical MOSFETs to establish a strip MAGFET with high biasing current [8]. In the absence of the applied magnetic induction B_Z , two drain currents, I_{D1} and I_{D2} , are the same at D1 and D2 of the MOSFETs, M1 and M2, respectively. After passing through the readout circuit, which includes a current-to-voltage (I-to-V) converter, a low-pass filter (LPF), and a difference amplifier (DA), the output voltage V_{OUT} of the DA is constant. That is, $\Delta V_{OUT} = 0$. By contrast, the output voltage V_{OUT} is a function of the bias current versus applied magnetic induction.

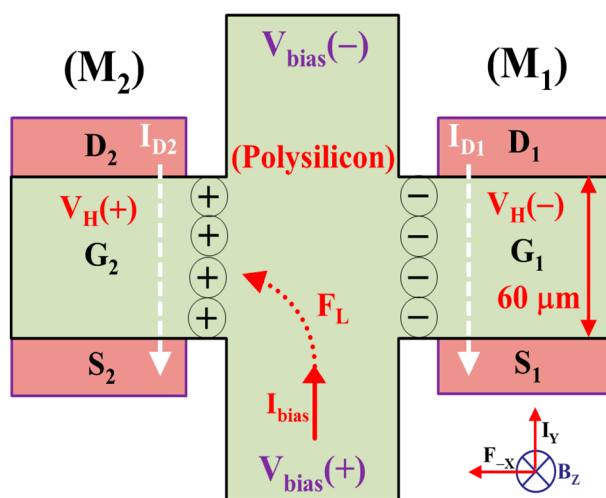


Figure 1. Strip MAGFET with two separated MOSFETs and a differential polysilicon CSHP. The Lorentz force F_L not only pushes the positive charge \oplus to the left to gather at the left side of the polysilicon CSHP, but also injects the electron current \ominus into the right side of the polysilicon CSHP to reduce the drain current of the first MOSFET (I_{D1}).

In general, the voltage-mode Hall devices can be biased in two modes: voltage biasing and current biasing. In the current biasing mode, the current-related sensitivity S_{RI} is calculated as follows [23]:

$$S_{RI}(B) = \left| \frac{1}{I_{bias}} \frac{\Delta V_{OUT}}{\Delta B} \right| \quad (1)$$

where the unit of $S_{RI}(B)$ is $V \cdot A^{-1} \cdot T^{-1}$, I_{bias} represents the supply bias current, ΔB represents the change in the applied magnetic induction, and ΔV_{OUT} represents a variation in the DA output voltage [23]. However, the proposed strip MAGFET detects the distance ΔD between the magnetic sensor and magnetic body. Thus, the current-related sensitivity should be redefined as follows:

$$S_{RI}(D) = \left| \frac{1}{I_{bias}} \frac{\Delta V_{OUT}}{\Delta D} \right| \quad (2)$$

where the unit of $S_{RI}(D)$ is $V \cdot A^{-1} \cdot m^{-1}$. In addition, the nonlinearity error (NLE) is defined as

$$NLE = \left| \frac{\Delta V_{OUT} - \Delta V_{OUT}^{(0)}}{\Delta V_{OUT}^{(0)}} \right| \times 100\% \quad (3)$$

where the unit of NLE is % and $\Delta V_{OUT}^{(0)}$ represents the calculated output voltage difference based on the slope of the straight line obtained from the best fit to the output characteristic [24]. The operational principle of the strip MAGFET is described below.

As shown in Figure 1, two identical MOSFETs, M_1 and M_2 , are operated in the saturation mode. If a magnetic induction B_Z and a bias current I_{bias} are applied to the polysilicon CSHP, the positive and negative Hall voltages, $V_H(+)$ and $V_H(-)$, are generated by Lorentz force F_L in the x -direction reversely and x -direction, respectively. In other words, the gate voltage of M_2 is larger than that of M_1 . By grounding two sources, S_1 and S_2 , two drain currents, I_{D1} and I_{D2} , can be expressed as follows:

$$\begin{cases} I_{D1} = \frac{1}{2}\mu_n C_{ox} \frac{W}{L} (V_{GS1} - V_{TH})^2 \\ I_{D2} = \frac{1}{2}\mu_n C_{ox} \frac{W}{L} (V_{GS2} - V_{TH})^2 \end{cases} \quad (4)$$

and

$$V_{GS2} - V_{GS1} = V_H(+)-V_H(-) = V_H \quad (5)$$

$$\frac{V_{GS1} + V_{GS2}}{2} = V_{GS} \quad (6)$$

where μ_n , C_{ox} , W , L , and V_{TH} represent the mobility of electrons, parasitic capacitance per unit gate area, width, length, and threshold voltage, respectively. V_{GS1} and V_{GS2} represent the differential gate-to-source voltages of M_1 and M_2 , respectively, with magnetic induction, whereas V_{GS} represents the gate-to-source voltage without magnetic induction. Subsequently, the induced Hall voltage V_H is derived from the Lorentz force.

$$V_H = G R_H I_{bias} B_Z / t \quad (7)$$

where $R_H = -\mu_n^* / \sigma_n = -r_n / nq$ represents the Hall coefficient, I_{bias} represents the bias current in the y -direction, B_Z represents the magnetic induction in the z -direction, and t and G represent the polysilicon thickness and geometrical correction factor, respectively [24]. Thus, the current difference between I_{D1} and I_{D2} can be expressed as follows:

$$\Delta I_D = I_{D2} - I_{D1} = \frac{1}{2}\mu_n C_{ox} \frac{W}{L} \left[2 \left(\frac{V_{GS1} + V_{GS2}}{2} - V_{TH} \right) (V_{GS1} - V_{GS2}) \right] \quad (8)$$

Rewriting Equation (8), we have

$$\Delta I_D = \mu_n C_{ox} \frac{W}{L} \times (V_{GS} - V_{TH}) V_H = \mu_n C_{ox} \frac{W}{L} \left(\frac{G R_H I_{bias} B_Z}{t} \right) (V_{GS} - V_{TH}) \quad (9)$$

As shown in Equation (9), the current difference ΔI_D is directly proportional to the bias current I_{bias} and the magnetic induction B_Z . If the bias current I_{bias} is set as constant, the larger the magnetic induction B_Z is, the higher the drain current difference ΔI_D is. The physical mechanism may be that the Lorentz force F_L pushes the positive charge to the left to gather at the left side of the polysilicon CSHP, which is connected to the gate terminal G_2 of the second MOSFET (M_2). Moreover, the electron current is directly injected into the right side of the polysilicon CSHP, which is connected to the gate node G_1 of the first MOSFET (M_1), to reduce the drain current of the first MOSFET (I_{D1}). By applying a magnetic induction (\sim mT) to the magnetic sensor, an output voltage V_{OUT} is acquired at the output node of the readout circuit by multiplying the drain current difference ΔI_D with a resistor R_D in the I-to-V converter and then multiplying approximately 16 times by $R_A = 100$ k Ω and $R_B = 6.2$ k Ω .

3. Readout Circuit

Two drain currents, I_{D1} and I_{D2} , obtained at two separated drains of two MAGFETs over the considered magnetic induction range, are of the order of few milliamperes (mA). By passing through the I-to-V converter with resistor R_D and LPF with resistor R_1 and capacitor C_1 , the high-frequency noise will be filtered out before the entering the DA. Figure 2 presents the readout circuit of the

proposed distance detector, which includes the I-to-V converter, LPF, and DA. Notably, the offset voltage can be effectively removed using the DA, and the single output V_{OUT} obtained is easy to use.

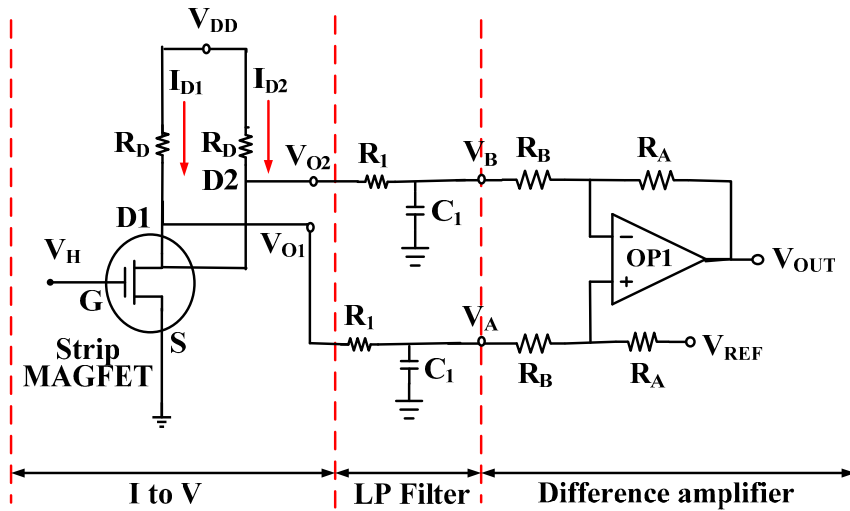


Figure 2. Readout circuit of the proposed distance detector comprising an I-to-V converter, low-pass filter (LPF), and difference amplifier (DA).

As shown in Figure 2, an I-to-V converter was selected to convert the induced drain current, obtained from the proposed strip MAGFET, into a Hall voltage with drain resistor R_D . Two output voltages, V_{O1} and V_{O2} , of the I-to-V converter can be expressed as follows:

$$\begin{cases} V_{O1} = V_{DD} - I_{D1} \times R_D \\ V_{O2} = V_{DD} - I_{D2} \times R_D \end{cases} \quad (10)$$

where V_{DD} represents the power supply. The output voltage of the DA, V_{OUT} , passing through the LPF with resistor R_1 and capacitor C_1 , is given by

$$V_{OUT} = V_{REF} - \Delta I_D \times R_D \times \left(\frac{1}{1 + sR_1C_1} \right) \times \frac{R_A}{R_B} \quad (11)$$

where V_{REF} represents a constant reference voltage, which is used to adjust the output level. $\Delta I_D (= I_{D1} - I_{D2})$ is defined as the drain current difference between the first and second drains of the MAGFET. For a DC magnetic induction, $s = 0$, the small-signal output voltage v_{out} is given by

$$v_{out} = -\Delta I_D \times R_D \times \frac{R_A}{R_B} \quad (12)$$

Figure 3 presents a low-voltage two-stage cascaded operational amplifier (opamp) with Miller compensation and compact class-AB output stage, which is composed of two common-source-connected output transistors, M_{19} and M_{20} [25]. To make the quiescent current of the output transistors insensitive to supply voltage variations, the floating current source should have the same supply voltage dependency as the class-AB control. The value of the current source is set using two bias voltages, V_{b5} and V_{b6} . The mirrors, M_7 – M_{10} and M_{15} – M_{18} , are loaded with the drain currents of the input pairs M_2 – M_3 and M_5 – M_6 , respectively. These drain currents and the gate–source voltages of M_7 and M_{17} change the common-mode input voltage. By adjusting two input bias currents with two bias voltages, V_{b1} and V_{b2} , the common-mode input voltage approaches the positive supply rail or the negative supply rail. The opamp is compensated by using the conventional Miller technique

including the cascode stages, M_{12} and M_{14} , in the Miller loops. This compensation technique shifts the output pole to a frequency of approximately [25].

$$\omega_{out} = \frac{C_M}{C_{GS,out}} \times \frac{g_{m0}}{C_L} \quad (13)$$

where g_{m0} represents the transconductance of the output transistors and C_L represents the load capacitor. C_M and $C_{GS,out}$ represent the total Miller capacitor and the total gate–source capacitance of the output transistor, respectively.

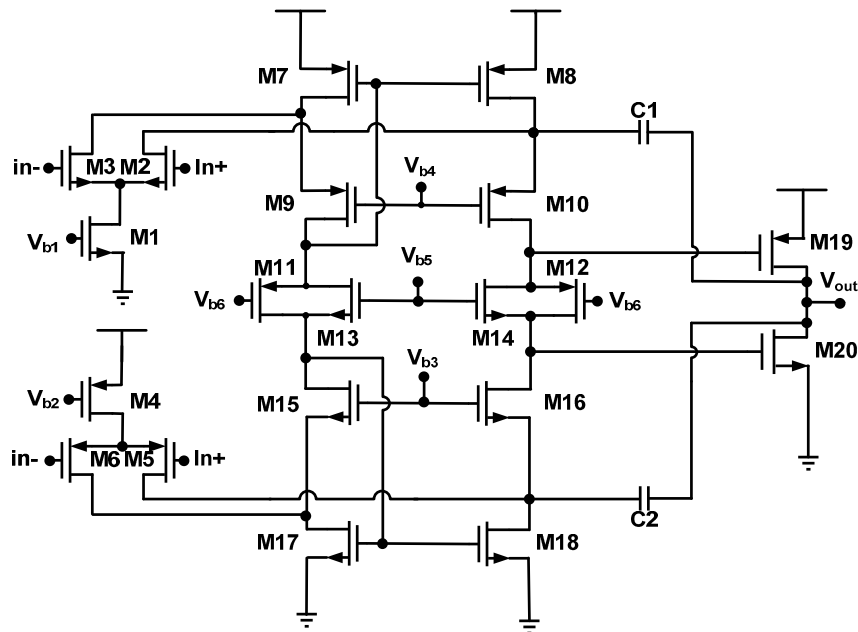


Figure 3. Low-voltage two-stage cascaded operational amplifier with Miller compensation and compact class-AB output stage.

Figure 4 presents the experimental setup of the distance detector composed of a device under test (DUT), an IA (INA333, Texas Instruments, Dallas, TX, USA) printed circuit board (PCB), a digital multimeter (Agilent 34405A, Santa Clara, CA, USA), a magnetic body (human), and a power regulator with a 9-V battery. The DUT included the strip MAGFET and readout circuit, and the magnetic body was actually a human weighing approximately 65 kg. The distance was defined from the chip center of the DUT to the weight center of the magnetic body. Notably, the proposed distance detecting method is not only a universal detection method but also operates in dark conditions away from light emission. To enhance the sensitivity of the distance detection and to increase the detecting distance, a commercial IA (INA333) was applied to amplify the output voltage of the readout circuit. Figure 5 presents the applied PCB that includes two commercial IAs, two bias voltages for IAs, two bias voltages for the proposed strip MAGFET, and resistors, R_C and R_D . By adjusting the variable resistor R_D , the magnifying power of IA1 was set to 43 dB (approximately 150 times).

Figures 6 and 7 present the measured equipment that includes a magnetic induction generator, a commercial IA (INA333) PCB, and a display monitor. As shown in Figure 6, only the offset voltage was displayed on the monitor and not the magnetic body. When the magnetic body contacts with the distance detector, Hall voltage evidently appeared on the monitor, as shown in Figure 7. A quality analysis of the measured Hall voltage is presented in Figure 7. To avoid bias, a digital multimeter (Agilent 34405A) was used for the quantity analysis of the distance detector that included a strip MAGFET, readout circuit, and IA PCB (INA333).

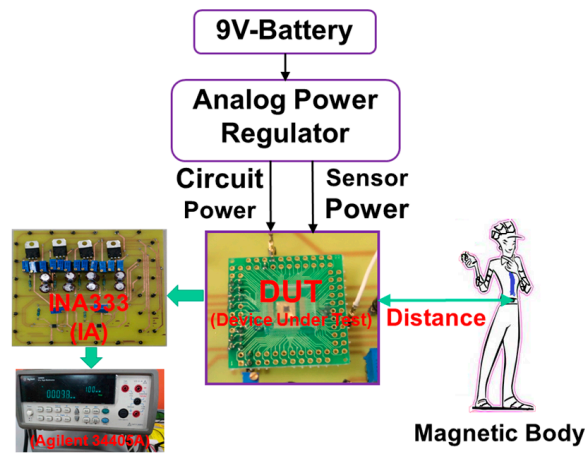


Figure 4. Experimental setup of distance detection.

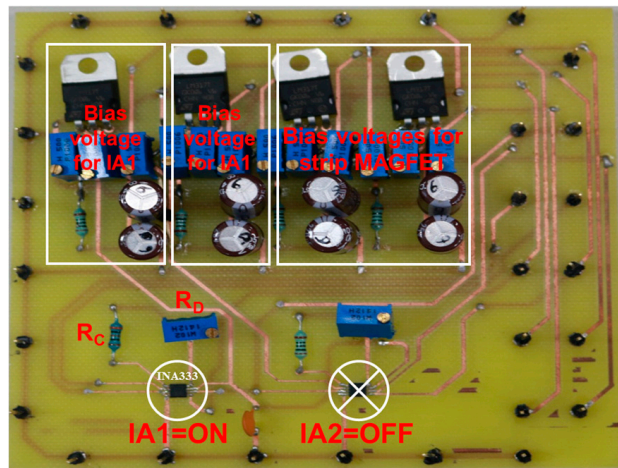


Figure 5. Applied PCB with two commercial instrumentation amplifiers (INA333).



Figure 6. Offset voltage (right circle) displayed on the monitor without a magnetic body and DUT (Device under test) placed in the magnetic induction generator.



Figure 7. Hall voltage appears on the monitor evidently when the magnetic body comes in contact with the distance detector.

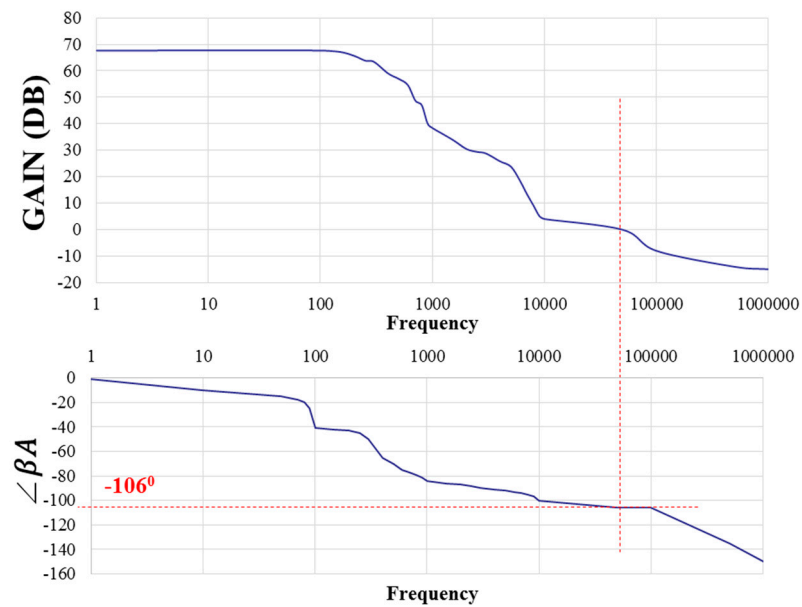
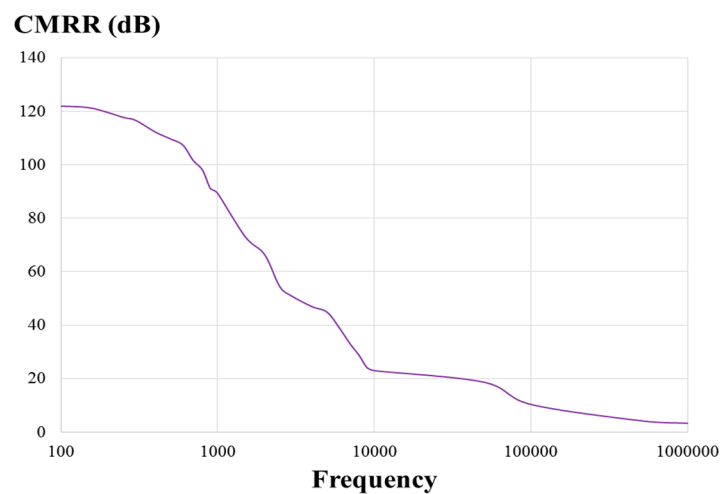
4. Simulated and Measured Results

This paper presents a low-voltage two-stage cascaded opamp with Miller compensation and compact class-AB output stage based on $0.18 \mu\text{m}$ CMOS technology for distance detection [25]. The simulated results demonstrated that the designed two-stage cascaded opamp had an open-loop gain of 75.3 dB, a phase margin of 54.9° , a common-mode rejection ratio (CMRR) of 123 dB, a slew rate of $0.07 \text{ V}/\mu\text{s}$, an input common-mode range (ICMR) of 0.9 V, a power supply rejection ratio (PSRR) of 119 dB, an output swing of 1.70 V, power consumption of $179 \mu\text{W}$ for a power supply of 1.8 volts, and a load capacitor of 10 pF.

Figure 8 presents a measured open-loop gain of 67.7 dB and phase of 74° with respect to frequency. The measured open-loop gain was lower than that obtained through simulation, but the measured phase was higher than that obtained through simulation. Figures 9 and 10 present the measured CMRR and PSRR, respectively, which were approximately equal to the relative simulated results. Furthermore, Figure 11 presents a measured slew rate of $0.07 \text{ V}/\mu\text{s}$, rise time of $19.73 \mu\text{s}$, and fall time of $6.67 \mu\text{s}$ at an operating frequency of 1 kHz. The simulated and measured results compared with those of previous studies are tabulated in Table 1. Measured results of voltage gain, phase margin, CMRR, slew rate, ICMR, PSRR, and output swing, were more favorable than those obtained in previous studies [26,27]. Although these previous studies have not proved the efficiency, the measured data in the present study verified that the designed opamp worked as intended. Figure 12 presents the microphotograph of the designed opamp without external resistors and capacitors. Notably, an output voltage V_{OUT} was acquired at the output node of the DA by multiplying the drain current difference ΔI_D with external resistors, $R_A = 100 \text{ k}\Omega$ and $R_B = 6.2 \text{ k}\Omega$. That is, the voltage gain of the DA was approximately 17 times greater.

Table 1. Comparison of simulated and measured results of amplifier with results of previous designs.

Specifications	This Work		[26]	[27]
	Simulation	Measurement	Simulation	Simulation
Technology	0.18 μm	0.18 μm	0.18 μm	0.5 μm
Voltage gain (dB)	75.3	67.7	67.7	45
Phase margin ($^\circ$)	54.9	74	-	-
CMRR (dB)	123	122	92	75
Slew rate (V/ μs)	0.07	0.07	-	-
ICMR (V_{PP})	0.9	0.744	-	-
Gain bandwidth (kHz)	1.85	0.225	1.75	5.8
UGB (MHz)	7.85	-	91.33	-
PSRR(+) (dB)	119	123	-	-
Output swing (V)	1.70	1.32	-	-
Power dissipation (μW)	179	274	263	280
Chip area (mm^2)	0.0153	0.0153	1.49	-

**Figure 8.** Measured open-loop gain of 67.7 dB and phase of 74° versus frequency (Hz).**Figure 9.** Measured common-mode rejection ratio (CMRR) of the designed opamp.

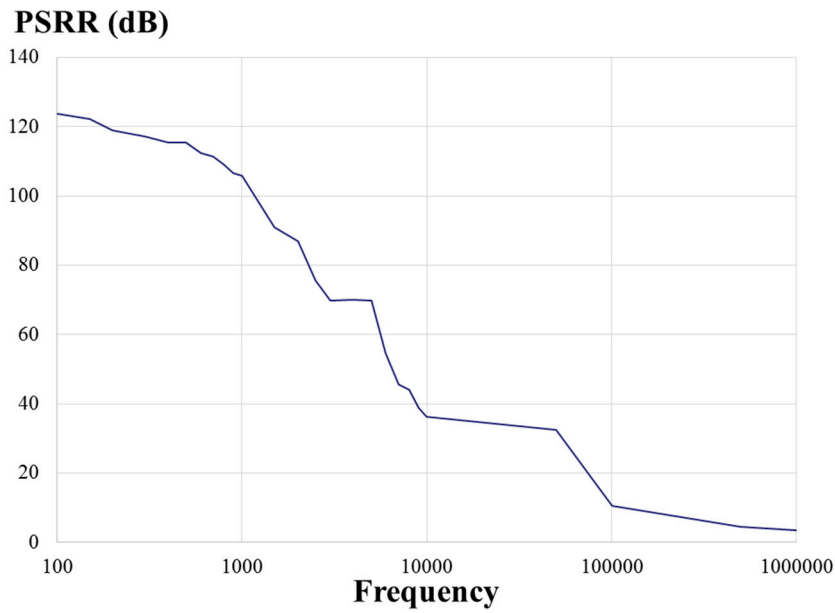


Figure 10. Measured power supply rejection ratio (PSRR) of the designed opamp with respect to frequency (Hz).

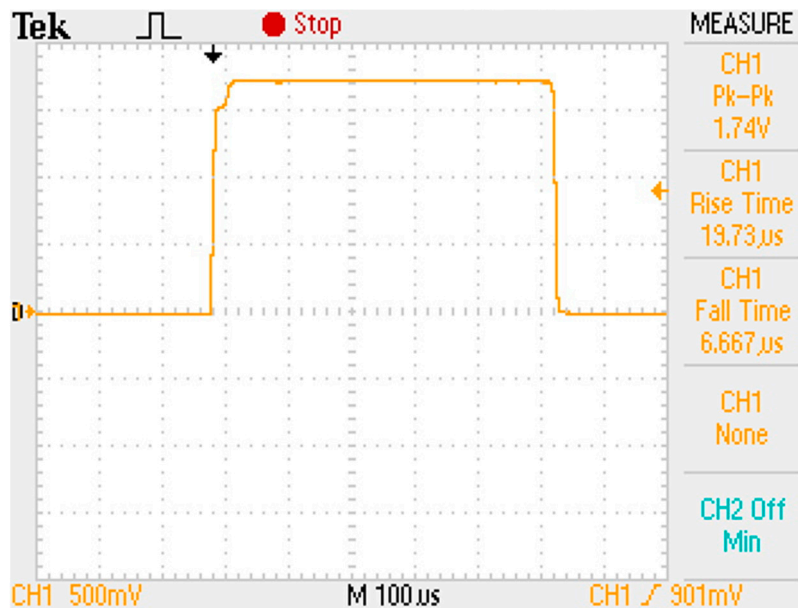


Figure 11. Measured slew rate of $0.07 \text{ V}/\mu\text{s}$, rise time of $19.73 \mu\text{s}$, and fall time of $6.67 \mu\text{s}$ at an operating frequency of 1 kHz.

To elucidate the detection mechanism, the experimental setup can be divided into three categories: direct measurement without grounding (direct), grounding to earth with electrostatic discharge (ESD) wrist strap (Strap E-GND), and grounding to power supply with ESD wrist strap (Strap S-GND). The first category elucidates the influence of ESD without grounding. Next, ESD will be eliminated from the magnetic sensor by grounding it to earth. Finally, in the third category, the ESD wrist strap is grounded to the power supply, and not to earth. This connection will enable the removal of ESD from the magnetic sensor to the power supply; however, ESD always exists between the power supply and earth.

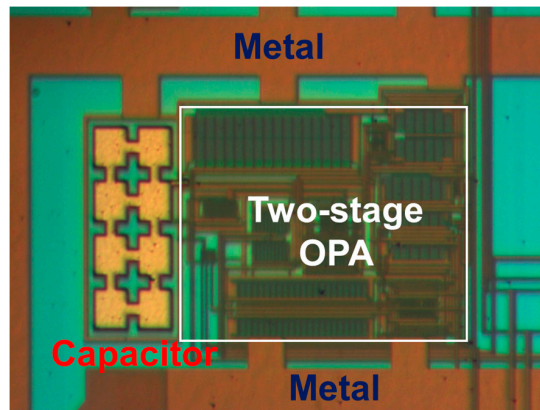


Figure 12. Microphotograph of the designed low-voltage two-stage cascaded opamp without external resistors and capacitors.

Figure 13 presents the measured output Hall voltages as a function of the distance, from 0 cm to 120 cm in steps of 10 cm, at a CSHP bias current (I_{bias}) of 12 mA. In the first category, the measured output Hall voltage varied from 58.35 to 59.00 mV. The voltage variation was approximately 0.65 mV. In the second category, the variation in the measured output Hall voltage was approximately 5.04 mV, from 57.54 to 62.58 mV. In the third category, the variation in the measured output Hall voltage was approximately 3.12 mV, from 60.58 to 63.70 mV. According to the measured Hall voltage, the second category performed with a more efficient sensitivity than the other two, and the first category performed with minimum sensitivity of nearly zero. That is, ESD could be eliminated from the magnetic sensor by grounding it to earth; however, ESD will cancel the sensitivity out when the sensor is not grounded. Notably, saturation was observed in the second category. This result indicates that the magnetic influence can be ignored if the human stayed far from the DUT, which was grounded to earth by using the ESD wrist strap (Strap E-GND). However, the first and third categories were still influenced by the magnetic body (human). Both ‘no grounding’ and ‘grounding to power supply’ were unsuitable for measuring the induced Hall voltage although the magnetic body was far and away from the designed DUT.

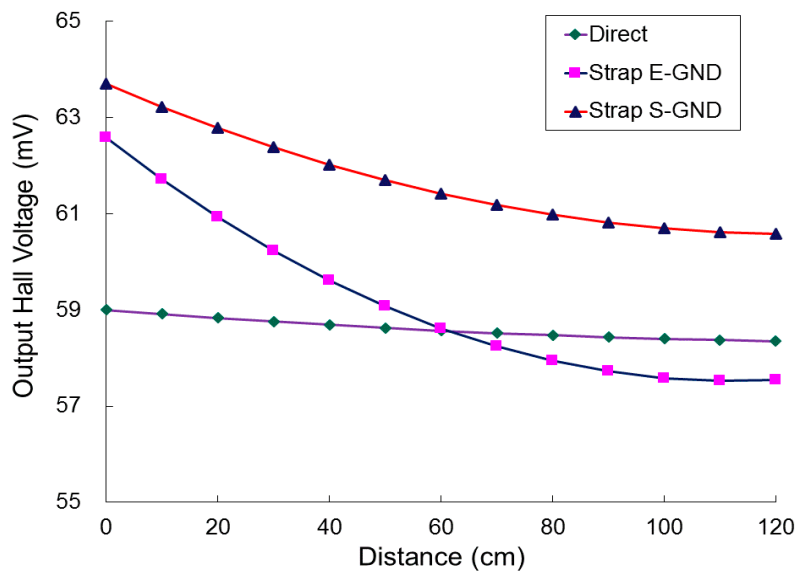


Figure 13. Measured output Hall voltages as a function of the distance, from 0 to 120 cm in steps of 10 cm, at a bias current of 12 mA for the proposed strip MAGFET with readout circuit and IA PCB (INA333).

Figure 14 presents the measured NLE as a function of distance, from 0 to 120 cm in steps of 10 cm, and various categories for the designed strip MAGFET with a readout circuit and an IA PCB. The variation in NLE was large when the MAGFET was operated in category 2 conditions in which the measurement is completed by grounding the sensor to earth with an ESD wrist strap (Strap E-GND). NLE was nearly constant when the measurement was finished without grounding. The sensor performed with a linear characteristic when operated in category 1, but yielded a quadratic curve in categories 2 and 3. Notably, NLE was equal to zero at two distances, 20 and 100 cm. The measured output voltage difference ΔV_{OUT} was equal to the calculated output voltage difference $\Delta V_{OUT}^{(0)}$ on the basis of the slope of the straight line obtained from the best fit to the output characteristic [24].

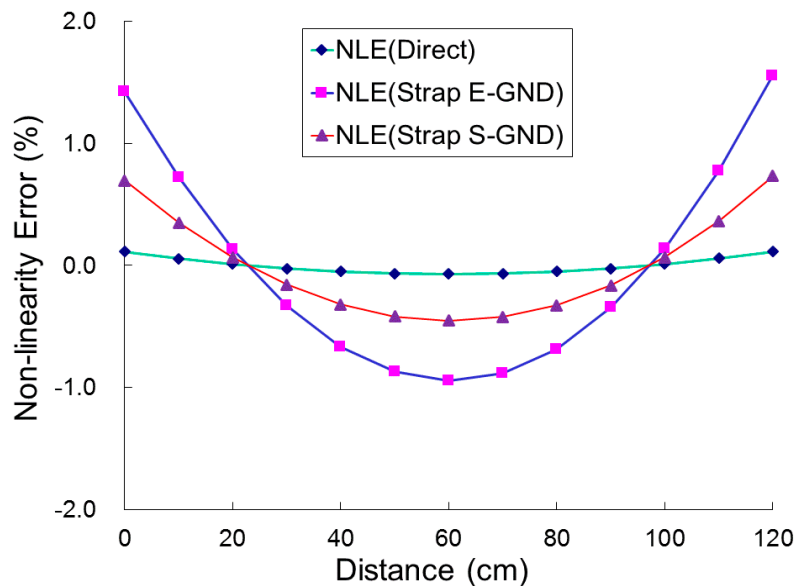


Figure 14. Measured nonlinearity errors (NLE) in categories 1, 2, and 3, against the distance, from 0 to 120 cm in steps of 10 cm, for the proposed strip MAGFET with a readout circuit and an IA PCB (INA333).

Table 2 summarizes the measured results of the proposed strip MAGFET with a readout circuit and an IA PCB (INA333). The average nonlinearity NLE_{ave} and the maximum nonlinearity NLE_{max} were proportional to the measured Hall voltage difference ΔV_H and the current-related sensitivity $S_{RI}(D)$ with a bias current of 12 mA. The maximum current-related magnetosensitivity was 0.35 V/A·m at an output Hall voltage of 5.04 mV and a distance of 0 cm (i.e., the magnetic body contacts with DUT). The measured results demonstrated that the proposed strip MAGFET was an effective distance sensor; however, it presented poor linearity. Figure 15 presents a microphotograph of the proposed strip MAGFET with a chip area of approximately $100 \times 220 \mu\text{m}^2$.

Table 2. Measurements of maximum output Hall voltages.

Category	ΔV_H (mV)	$S_{RI}(D)$ (V/A·M)	NLE_{ave} (%)	NLE_{max} (%)	I_{bias} (mA)	Distance (cm)	Grounded Mode
1	0.65	0.045	0.055	0.112	12	120	Direct
2	5.04	0.350	0.729	1.426	12	120	Strap E-GND
3	3.12	0.217	0.349	0.732	12	120	Strap S-GND

ΔV_H ; optimum current-related magnetosensitivities, $S_{RI}(D)$; average nonlinearity error, NLE_{ave} ; maximum nonlinearity error, NLE_{max} ; and maximum distance at a bias current of 12 mA for the proposed strip MAGFET with a readout circuit and an IA PCB.

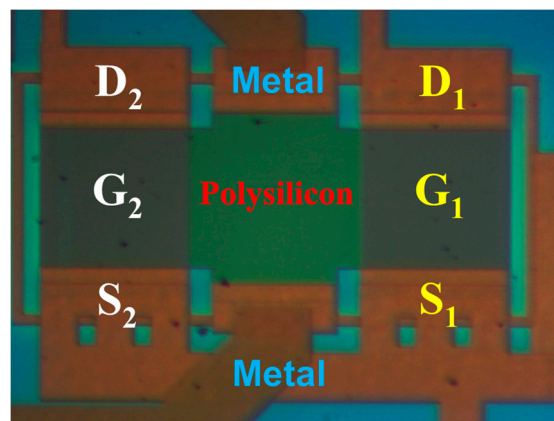


Figure 15. Microphotograph of the proposed strip MAGFET comprising two separated MOSFETs and a differential polysilicon cross-shaped Hall plate (CSHP).

5. Conclusions

In this paper, a strip MAGFET with a readout circuit and an IA PCB (INA333) is presented to measure the distance from a magnetic body (human) to the DUT, which was fabricated using 0.18 μm 1P6M CMOS technology. The object to be measured cannot be detected using the proposed magnetic sensor if the object is located in the dark or has diverged from the oriental range even when the object is considerably closer to the sensor. The physical mechanism underlying this phenomenon is that the Lorentz force pushes the positive charge to the left to gather at the left side of the polysilicon CSHP, which is connected to the gate terminal of the second MOSFET (M_2). The current difference ΔI_D between the two drains will be amplified linearly. After passing through the readout circuit, the magnetosensitivity of the sensor will be improved effectively by amplifying the current difference ΔI_D . The experimental results revealed that ESD could be eliminated from the magnetic sensor by grounding the sensor to earth; however, the magnetosensitivity is canceled out without grounding. Furthermore, the magnetic influence can be ignored if the human stays far from the DUT, which is grounded to earth by using the ESD wrist strap (Strap E-GND). Both 'no grounding' and 'grounding to power supply' were unsuitable for measuring the induced Hall voltage of the magnetic body. Notably, the *NLE* was nearly constant when the measurement was completed without grounding. The sensor performed with a linear characteristic in category 1, whereas yielded a quadratic curve in categories 2 and 3. The maximum current-related magnetosensitivity of 0.35 V/A·m was obtained at an output Hall voltage of 5.04 mV and a distance of 0 cm (i.e., the magnetic body was in contact with the DUT). According to the measured results, the proposed strip MAGFET with a readout circuit and an IA PCB (INA333) is an efficient distance detector. Moreover, this study is unique because it compensates for the lack of the research literature in Open Access Publishing related to distance detection by using a magnetic sensor.

Acknowledgments: The authors would like to thank the Ministry of Science and Technology, R.O.C., for financially supporting this research under Contract No. MOST 103-2622-E-027-014-CC3. They are grateful to the Chip Implementation Center (CIC), Taiwan, for fabricating the test chip. Jane Nicholson is appreciated for her editorial assistance.

Author Contributions: This study was completed with three contributors. G.-M.S. designed the magnetic device, completed the theoretical analysis, and wrote the paper; W.-S.L. conceived and designed the experiments; H.-K.W. analyzed the data and surveyed the references.

Conflicts of Interest: The authors declare no conflict of interest.

References

1. Henriksen, D.; Dalslet, B.T.; Skieller, D.H.; Lee, K.H.; Okkels, F.; Hansen, M.F. Planar Hall effect bridge magnetic field sensors. *Appl. Phys. Lett.* **2010**, *97*. [[CrossRef](#)]
2. Heidari, H.; Gatti, U.; Bonizzoni, E.; Maloberti, F. Low-noise low-offset current-mode Hall sensors. In Proceedings of the 9th Conference on Ph.D. Research in MicroElectronics and Electronics (PRIME 2013), Villach, Austria, 24–27 June 2013; pp. 325–328.
3. Nathan, I.A.; Mckay, I.; Filanovsky, M.; Baltes, H.P. CMOS oscillator with magnetic-field frequency modulation. *IEEE J. Solid State Circuits* **1987**, *22*, 230–232. [[CrossRef](#)]
4. Heidari, H.; Bonizzoni, E.; Gatti, U.; Maloberti, F. A 0.18- μm CMOS current-mode Hall magnetic sensor with very low bias current and high sensitive front-end. In Proceedings of the 2014 IEEE Sensors, Valencia, Spain, 2–5 November 2014; pp. 1467–1470.
5. Ajbl, A.; Pastre, M.; Kayal, M. A fully integrated Hall sensor microsystem for contactless current measurement. *IEEE Sens. J.* **2013**, *13*, 2271–2278. [[CrossRef](#)]
6. Pastre, M.; Kayal, M.; Blanchardl, H. A Hall sensor analog front end for current measurement with continuous gain calibration. *IEEE Sens. J.* **2007**, *7*, 860–867. [[CrossRef](#)]
7. Min, Y.J.; Kwon, C.K.; Kim, H.K.; Kim, C.; Kim, S.W. A CMOS magnetic Hall sensor using a switched biasing amplifier. *IEEE Sens. J.* **2012**, *12*, 1195–1196. [[CrossRef](#)]
8. Donoval, M.; Daricek, M.; Stopjakova, V.; Donoval, D. Magnetic FET-based on-chip current sensor for current testing of low-voltage circuits. *J. Electr. Eng.* **2008**, *59*, 122–130.
9. Yunruo, Y.; Dazhong, Z.; Qing, G. Sector split-drain magnetic field effect transistor based on standard CMOS technology. *Sens. Actuators A Phys.* **2005**, *121*, 347–351. [[CrossRef](#)]
10. Castaldo, F.C.; Mognon, V.R.; dos Reis Filho, C.A. Magnetically cupled current sensors using CMOS split-drain transistors. *IEEE Trans. Power Electron.* **2009**, *24*, 1733–1736. [[CrossRef](#)]
11. Torres, R.R.; Dominguez, E.A.G.; Klima, R.; Selberherr, S. Analysis of split-drain MAGFETs. *IEEE Trans. Electron Devices* **2004**, *51*, 2237–2245. [[CrossRef](#)]
12. Sung, G.M.; Yu, C.P. 2-dimensional differential folded vertical Hall device fabricated on a p-type substrate using CMOS technology. *IEEE Sens. J.* **2013**, *13*, 2253–2262. [[CrossRef](#)]
13. Mccall, W.D.; Rohan, E.J. A linear position transducer using a magnet and Hall effect devices. *IEEE Trans. Instrum. Meas.* **1977**, *26*, 133–136. [[CrossRef](#)]
14. Arcire, A.; Mihalache, G. Position control of a bidirectional moving magnet actuator based on contactless Hall-effect transducer. In Proceedings of the 9th International Symposium on Advanced Topics in Electrical Engineering, Bucharest, Romania, 7–9 May 2015; pp. 417–421.
15. Netzer, Y. A very linear noncontact displacement with a Hall-element magnetic sensor. *Proc. IEEE* **1981**, *69*, 491–492. [[CrossRef](#)]
16. Sugimoto, T.; Suzuki, K.; Dohmeki, H. A position detecting method using Hall element for discontinuous stator permanent magnet linear synchronous motor. In Proceedings of the XIX International Conference on Electrical Machines (ICEM 2010), Rome, Italy, 6–8 September 2010; pp. 1–6.
17. Chen, B.; Lu, G.; Hao, R.; Hu, L.; Tian, X. Intelligent speed and mileage measurement system for vehicles based on Hall sensor. In Proceedings of the 2009 First International Workshop on Education Technology and Computer Science, Wuhan, China, 7–8 March 2009; pp. 272–274.
18. Hernandez, D.C.; Filonenko, A.; Seo, D.; Jo, K.H. Laser scanner based heading angle and distance estimation. In Proceedings of the 2015 IEEE International Conference on Industrial Technology (ICIT), Seville, Spain, 17–19 March 2015; pp. 1718–1722.
19. Jankowski, S.; Szymanski, Z.; Dziomin, U.; Mazurek, P.; Wagner, J. Deep learning classifier for fall detection based on IR distance sensor data. In Proceedings of the 2015 IEEE 8th International Conference on Intelligent Data Acquisition and Advanced Computing Systems, Technology and Applications (IDAACS), Warsaw, Poland, 24–26 September 2015; pp. 723–727.
20. Qian, H.M.; Zhou, J.; Yuan, Y. Visual-based fall detection using histogram of oriented gradients of Poisson distance image. In Proceedings of the 2015 Chinese Automation Congress (CAC), Wuhan, China, 27–29 November 2015; pp. 657–662.

21. Zhao, M.; Mammeri, A.; Boukerche, A. Distance measurement system for smart vehicles. In Proceedings of the 2015 7th International Conference on New Technologies, Mobility and Security (NTMS), Paris, France, 27–29 July 2015; pp. 1–5.
22. Rezaei, N.; Dehghani, R.; Jalili, A.; Mosahebfard, A. CMOS magnetic sensor with MAGFET. In Proceedings of the 2013 21st Iranian Conference on Electrical Engineering (ICEE), Mashhad, Iran, 14–16 May 2013; pp. 1–5.
23. Baltes, H.P.; Popovic, R.S. Integrated semiconductor magnetic field sensors. *Proc. IEEE* **1986**, *74*, 1107–1132. [[CrossRef](#)]
24. Roumenin, C.S. Bipolar magnetotransistor sensors: An invited review. *Sens. Actuators A Phys.* **1990**, *24*, 83–105. [[CrossRef](#)]
25. Hogervorst, R.; Tero, J.P.; Eschauzier, G.H.; Huijsing, J.H. A compact power-efficient 3 V CMOS rail-to-rail input/output operational amplifier for VLSI cell libraries. *IEEE J. Solid State Circuits* **1994**, *29*, 1505–1513. [[CrossRef](#)]
26. Goel, A.; Singh, G. Novel high gain low noise CMOS instrumentation amplifier for biomedical applications. In Proceedings of the IEEE 2013 International Conference on Machine Intelligence and Research Advancement (ICMIRA), Jammu, India, 21–23 December 2013; pp. 392–396.
27. Goswami, M.; Khanna, S. DC suppressed high gain active CMOS instrumentation amplifier for biomedical application. In Proceedings of the IEEE 2011 International Conference on Emerging Trends in Electrical and Computer Technology (ICETECT), Nagercoil, India, 23–24 March 2011; pp. 747–751.



© 2017 by the authors; licensee MDPI, Basel, Switzerland. This article is an open access article distributed under the terms and conditions of the Creative Commons Attribution (CC-BY) license (<http://creativecommons.org/licenses/by/4.0/>).